PROCEEDINGS, Fourtieth Workshop on Geothermal Reservoir Engineering
Stanford University, Stanford, California, January 26-28, 2015
SGP-TR-204

Anomalous Solute and Heat Diffusion in Fault Structures

Anna Suzuki, Toshiyuki Hashida, Kewen Li and Roland N. Horne

Department of Energy Resources Engineering, 67 Panama Dr., Stanford, California, USA, 94305

anna3@stanford.edu

Keywords: tracer test, thermal response, fractional derivative, fractal

ABSTRACT

A structure associated with large-scale faults can contribute to control fluid flow in a geothermal reservoir. The fracture density at the damage zone in the fault zone decays with distance from the main conduit. A fractional advection-dispersion equation (fADE) and a fractional heat transfer equation (fHTE) describe diffusion processes of solute and heat into the surrounding rocks through fractal geometry and have been developed to characterize mass and heat transfer in the fault-related structure. This study conducted numerical simulation and column flow experiments to generate tracer responses and temperature profiles. The results reveal that permeability patterns in the surrounding rocks affect on the reservoir responses. Both numerical and experimental results simulating tracer response with a fault-related structure show a gradual decrease in concentration of tracer. The fADE and fHTE solutions were found to be in reasonable agreement with the tracer responses and the temperature profiles for a fault zone model.

1. INTRODUCTION

Fracture and fracture networks contribute importantly to tracer migration and heat propagation. In a geothermal reservoir, structures associated with large-scale faults appear to be quite important in controlling fluid flow (Massart et al., 2010). The simplest description of a fault structure (and fault zones in general) considers two major mechanical units, namely a fault core and a damage zone (cf., Caine et al., 1996; Faulkner et al., 2010). The fault core is formed through repeated slipping of the principal fault plane and is composed of impermeable barriers. In contrast, the damage zone consists of a volume of deformed rocks around a fault surface that results from the slips along faults (Caine et al., 1996). In the fault damage zone, the fracture density (the number of fractures per unit length) commonly increases near the fault core (e.g., Brock and Engelder, 1977; Chester and Logan, 1986; Agosta and Kirschner, 2003; De Joussineau and Aydin, 2007; Gudmundsson, 2011). Savage and Brodsky (2011) found that isolated single faults with small displacements have macrofracture densities that decay as a power law and that mature fault damage zones can be interpreted as a superposition of these power-law functions. A power-law function is a feature of fractal geometry, which provides widely applicable and descriptive tools for characterization of subsurface fracture systems (Bonnet et al., 2001).

Tracer testing is a standard method for evaluating fluid flow inside a geothermal reservoir. Fomin et al. (2005) derived an equation with fractional derivatives that accounts for the diffusion of solute into surrounding rocks using fractal geometry. The model enables reproduction of tracer responses, including the heavy tails often observed in geothermal tracer tests. In the last decade, many authors have made notable contributions to both the theory and the application of the fractional advection-dispersion equation (fADE) in hydrology, as reviewed by Zhang et al. (2009). The advantage of using the fADE is its ability to describe fluid flow based on a mathematical description of the fractal geometry (Fomin et al., 2011). Based on the concept of the fADE, the fractional heat transfer equation (fHTE) has been proposed to evaluate thermal response due to cold-water injection in a geothermal reservoir (Suzuki et al., 2014). The fHTE allows for the effect of thermal diffusion into surrounding rocks in the same manner as the fADE.

We studied the description of the spatial gradient of the fracture density at a fault damage zone by a power-law function. Because the fADE and the fHTE describe diffusion processes of solute and heat into the surrounding rocks through fractal geometry, they are expected to be suitable for characterizing mass and heat transfer in the fault-related structure. If the fracture distribution in a geothermal reservoir can be modeled successfully by a power-law fracture density, then the fADE and the fHTE would be useful for characterizing tracer and thermal response for the geothermal development. In this study, the effect of permeability distribution at a fault zone on tracer and thermal responses was demonstrated. A numerical reservoir simulator, TOUGH2, was used to generate reservoir performance data to verify the applicability of the fADE and the fHTE. An experiment was also designed to obtain insights into the behavior of tracers with the fault-associated structure.

2. MASS TRANSPORT AND HEAT TRANSFER AT A FAULT ZONE

2.1 Fracture density at a fault zone

According to field observations in geothermal reservoirs, it is known that usually the main permeable zones are composed of fault-related structures, which result from a complex set of components, such as a fault core and a damage zone (Caine et al., 1996). Savage and Brodsky (2011) suggested that the fracture density, *FD*, at a damage zone decays with distance from the faults according to a power law as follows:

$$FD = FD_0 r^{-n}, \quad (1)$$

where FD_0 is the constant of fracture density, r is the distance from the fault, and n is the exponent describing the decay.

Suzuki et al. (2015, submitted to for publication) evaluated whether the power-law model of fracture density is applicable to fault zone architectures in a geothermal reservoir. In the work by Brogi (2008), the structural architectures of 13 normal faults were investigated in the Rapolano geothermal area (hinterland of the Northern Apennines, Italy). The results showed the frequency distributions of fracture density in the Rapolano geothermal area decreased with the distance and could be fitted by power-law approximations. The power-law approximation of fracture density, which is written in Eq. (1), may be valid to characterize the fracture distribution in the fault-related structure in the geothermal reservoir.

2.2 Mass transport model

Fomin et al. (2011) proposed the one-dimensional advection-dispersion equation (fADE) to model solute transport in a fracture system. Detailed descriptions of the mass transport model can be found in the literature (Fomin et al. 2005, 2011). The fADE is capable of describing diffusion into the surrounding rocks by using a Caputo fractional derivative with respect to time, based on a diffusion equation formulated according to fractal geometry (Samko et al., 1993). The diffusion equation includes a fractal diffusion coefficient that decreases with distance according to a power law. When fracture density decreases with distance as described in Eq. (1), it is likely that the diffusion coefficient also changes spatially. In this study, the diffusion processes, which occur to the surrounding rocks from the main conduit perpendicular to the fault core, are described by the fractal diffusion coefficient taken into account in the fADE.

The schematic of a fractured reservoir for the fADE is represented in Fig. 2. All the fault zones are characterized by three architectural scales. The numbers of subscripts, i, for some variables represent the objective scales, respectively. At a larger scale (i = 1), a fault zone system consists of a fault core and damage zones, in which a main conduit with high permeability is formed along the fault core. At this scale, the major flow is assumed to be one dimensional, but diffusion into the surrounding rocks occurs. At an intermediate scale (i = 2), the main conduit is characterized by complex fracture networks inside the damage zone. At a smaller scale (i = 3), the rock matrix includes secondary branched fractures and minor faults.

$$\frac{\partial \phi_2 c_2}{\partial t} + a_3 \frac{\partial^{\gamma} c_2}{\partial t^{\gamma}} + a_1 \frac{\partial^{\beta} c_2}{\partial t^{\beta}} = D_2 \frac{\partial}{\partial x}\left(p \frac{\partial^{\alpha} c_2}{\partial x^{\alpha}} + (1-p) \frac{\partial^{\alpha} c_2}{\partial (-x)^{\alpha}} \right) - v \frac{\partial c_2}{\partial x} , \tag{2}$$

where t is time. x is distance from injection zone. c_2 and ϕ_2 are the concentration of tracer and the porosity in the main conduit, respectively. D_2 and v are the dispersion coefficient and the Darcy velocity in the main conduit, respectively. a_1 and a_3 are the retardation coefficient related to diffusion processes in the surrounding rocks and in the matrix, respectively. The skewness parameter is given by p (Huang et al. 2008). α ($0 < \alpha \leq 1$), β ($0 < \beta \leq 1$) and γ ($0 \leq \gamma \leq 1$) are the orders of the fractional temporal derivatives. In order to normalize Eq. (2), nondimensional variables and modified retardation coefficients are introduced as follows:

$$\tau = \frac{t}{t_{tracer}}, \quad X = \frac{x}{l}, \quad C = \frac{c_2}{c_0}, \quad Pe = \frac{vl^{a}}{D_2}, \quad b_1 = \frac{a_1}{\phi_2} t_{tracer}^{1-\beta} , \quad b_3 = \frac{a_3}{\phi_2} t_{tracer}^{1-\gamma} ; \tag{3}$$

where t_{tracer}, l and c_0 are the representative values of time, length, and concentration, respectively. In this study, the representative length, l, was set to the distance between the inlet and the outlet. The representative time, t_{tracer}, is the period that tracer migrates the distance, l, at the velocity, v. The representative concentration, c_0, is injected concentration of tracers. Pe is the Péclet number.

By using the above nondimensional variables, the normalized governing equation of Eq. (2) can be written as:

$$\frac{\partial C}{\partial \tau} + b_3 \frac{\partial^{\gamma} C}{\partial \tau^{\gamma}} + b_1 \frac{\partial^{\beta} C}{\partial \tau^{\beta}} = \frac{1}{Pe} \frac{\partial}{\partial x}\left(p \frac{\partial^{\alpha} C}{\partial X^{\alpha}} + (1-p) \frac{\partial^{\alpha} C}{\partial (-X)^{\alpha}} \right) - \frac{\partial C}{\partial X} . \tag{4}$$

Here, the first term on the left side of Eq. (4) is the accumulation term, and the second term models the retardation process associated with diffusion into matrix induced by secondary branched fractures. The third term describes the process of vertical diffusion into the surrounding rock masses. The first term on the right side expresses dispersion within the main conduit, and the second term is the advection term. When the values of b_1 and b_3 are set to 0 and the order of spatial fractional derivative α is set to 1, Eq. (4) is consistent with the conventional advection-dispersion equation (ADE) (Bear, 1972).

2.3 Heat transfer model

The analogous behaviors of heat and mass transfer have been long recognized (Welty et al., 2007). Because of this analogy, the fractal geometry taken into account in the fADE may lead to characterization of fractal thermal diffusion. The governing equation to model heat transfer in fractured media, which is called the fractional heat transfer equation (fHTE), has been derived as follows:

$$\frac{\partial}{\partial \tau} \overline{\rho C_{p2}} T_2 + d_3 \frac{\partial^{\gamma'} T_2}{\partial t^{\gamma'}} + d_1 \frac{\partial^{\beta'} T_2}{\partial t^{\beta'}} = - \frac{\partial \rho_w C_{pw2} v T_2}{\partial x} , \tag{5}$$

where: $\overline{\rho C}_{p2} = \phi_2 \rho_w C_{pw2} + (1-\phi_2)\rho_r C_{pr2}$; ρ_w and ρ_r are the density of water and rock, respectively; C_{pw2} and C_{pr2} are the heat capacity of water and rock in the main conduit; T_2 is temperature; The coefficients d_1 and d_3 represent retardation processes caused by the heat diffusivities into the surrounding rocks and into the matrix; β' ($0 < \beta \leq 1$) and γ' ($0 \leq \gamma \leq 1$) are the orders of the fractional derivatives. In Eq. (5), thermal conduction inside the reservoir is negligible, as indicated by Woods and Fitzgerald (1993). In Suzuki et al. (2014), the governing equation given by Eq. (5) was normalized by using the migration time of the heat front. This study aimed at connecting the fADE and the fHTE. Accordingly, the migration time of tracers, t_{tracer}, was used for normalization of Eq. (5). The variables are introduced as follows:

$$\tau = \frac{t}{t_{tracer}}, \quad X = \frac{x}{l}, \quad T = \frac{T_{pro} - T_{in}}{T_r - T_{in}}, \quad e_1 = \frac{d_1}{\overline{\rho C}_{p2}} t_{tracer}^{1-\beta'}, \quad e_3 = \frac{d_3}{\overline{\rho C}_{p2}} t_{tracer}^{1-\gamma'}; \tag{6}$$

where T_{pro} is the temperature of produced fluid at the outlet, T_r is the initial temperature of the reservoir, and T_{in} is the temperature of injected water. The normalized equation of the fHTE can be written in the following form:

$$\frac{\partial T}{\partial \tau} + e_3 \frac{\partial^{\gamma'} T}{\partial \tau^{\gamma'}} + e_1 \frac{\partial^{\beta'} T}{\partial \tau^{\beta'}} = -\frac{\phi_2 \rho_w C_{pw2}}{\overline{\rho C}_{p2}} \frac{\partial T}{\partial X}. \tag{7}$$

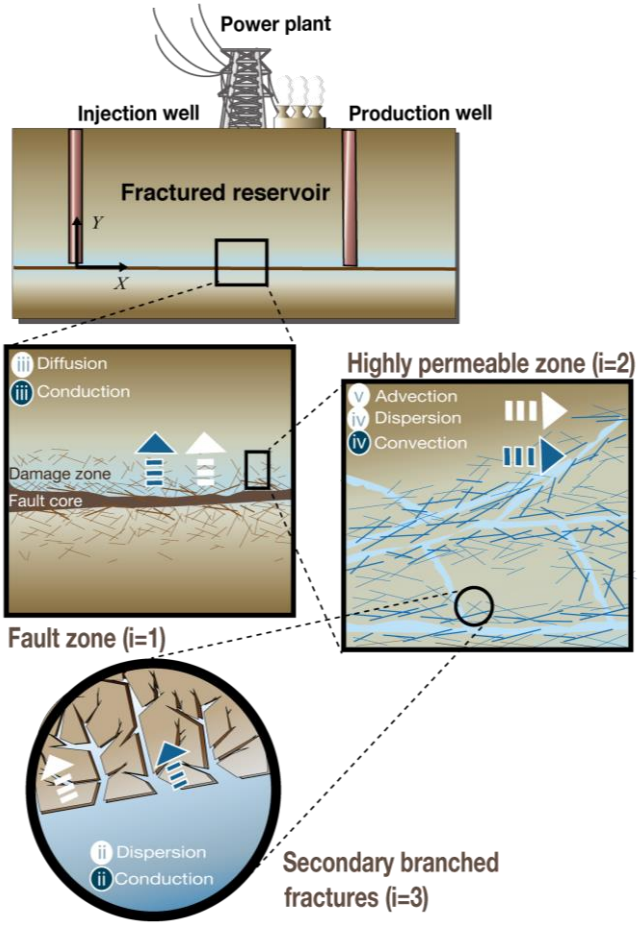

Figure 1: Schematic of a fractured reservoir.

3. NUMERICAL SIMULATION

3.1 Model description

A numerical reservoir simulator, TOUGH2, was used to generate synthetic field performance data to reveal influences of the structure in a fault zone and to verify the applicability of the fADE and the fHTE. The TOUGH2 simulation solves mass and energy balance

equations that describe fluid and heat flow in general multicomponent systems (Pruess, 1999). Figure 3 shows a schematic of the numerical simulation model. The numerical properties are summarized in Table 1. The reservoir was assumed to be homogeneous and to consist of a main conduit with high permeability and the surrounding rocks with low permeability. The thickness H and length L of the calculation domain were set to H = 20 m and L = 100 m, respectively. The main conduit is along a fault core, which is parallel to the x-axis. The thickness of the main conduit was set to H_0 = 0.1 m. A relatively fine grid was employed around the main conduit to resolve the flow. Grid size in the calculation domain was 1 m × 1 m except the main conduit and its vicinity refined by 1 m × 0.1 m. The discretization was determined to be fine enough because the simulation results had only small differences from the result using finer grids.

One-dimensional advective bulk flow travels from the injection zone towards the production zone. The tracer was injected for one day in the injection zone, after which the injection was switched to fresh water. Because the fADE and the fHTE described by Eqs. (4) and (7) are concerned with single-phase flow, fluid flow was simulated to be liquid phase. The initial temperature of the reservoir was 200 °C. The temperature of the tracer and the injected water was constant at 100 °C. The tracer response and temperature profile were observed in the production zone. Provided that the rock grains are sufficiently small and the fluid velocities sufficiently low, local thermodynamic equilibrium between the rock and fluid can be assumed. It was also assumed that the rock is incompressible, that both rock and fluid have constant thermal properties, and that tracer diffusion and thermal conduction in the main conduit were neglected. Permeability value in main conduit was set to $1.0\text{x}10^{-13}$ m^2. Porosity, rock density, and thermal conductivity were 0.1, 2500 kg/m^3 and 2.5 W/m^2 °C to all rocks, respectively. Rock parameters used in TOUGH2 are summarized in Table 3.

As mentioned in the previous section, the fracture density at a damage zone decays with distance from the faults according to a power law. In this study, the fracture density is expressed in terms of the permeability, which is taken to be a power law in the following form:

$$K_s(Y) = K_0(Y+1)^{-\theta}, \tag{8}$$

where K_0 and H_0 are the constant permeability and the thickness of the main conduit, respectively; Y is the distance from the main conduit; θ is the index of anomalous diffusion in the surrounding rocks.

For comparison, three different reservoir models were examined using TOUGH2: a one-layer model, a two-layer model and the fault zone model mentioned above. The most simplified model to capture the fractured nature of a geothermal reservoir is a one-layer model, in which fluid flow occurs through fractures surrounded by impermeable rock matrix (Bullivant and O'Sullivan, 1989). A two-layer model is an extension of the double-porosity concept, originally developed by Barenblatt et al. (1960) and Warren and Root (1963). The double-porosity concept is based on the notion that fractures have large transmissivity and low storativity, while the surrounding rocks have the opposite characteristics. Therefore, any disturbance in reservoir conditions will travel rapidly through the network of interconnected fractures, while invading the matrix blocks only slowly (Pruess and Narasimhan, 1982, 1985). The one-layer model and the two-layer model used the same rock parameters as the fault zone model summarized in Table 3. Permeability value in main conduit was set to $1.0\text{x}10^{-13}$ m^2. The surrounding area of the main conduit in the one-layer model is impermeable. The two-layer model has constant permeability in the surrounding area.

The tracer breakthrough and temperature histories obtained by TOUGH2 were used to match with the fADE and the fHTE. A finite difference approach discretized in time using an implicit method was used to solve the fADE and the fHTE (Suzuki et al. 2014). The tracer responses and thermal responses calculated using TOUGH2 were normalized using representative physical variables discussed in previous session. This study addressed the effect of structures of a fault zone, which probably leads to diffusion into the surrounding rocks. Thus, we used constitutive parameters in the third terms on the left-hand side in Eqs. (4) and (7). The effects of diffusion into the matrix, which can be described by the second terms on the left-hand side in Eqs. (4) and (7), and the heterogeneity inside the main conduit, which can be modeled by the first term on the right-hand side in Eq. (4), need further research. Therefore, b_3 and e_3 were set to 0, and α was set to 1. In addition, because it is known that p is less than 0.5 in the case where fluid flow within a reservoir is subject to preferential flow paths, this study set p to zero, which is consistent with other studies (i.e., Zhang et al., 2007). With respect to the fADE, the parameters required to fit the tracer data are b_1 and β, and Pe which are obtained from the root-mean-square error (RMSE):

$$RMSE = \sqrt{\frac{1}{N}\sum_{i=1}^{N}\left(C_i^{fADE} - C_i^{tracer}\right)^2}, \tag{9}$$

where N is the number of data points, C_i^{fADE} is the ith concentration calculated by the fADE, and C_i^{trace} is the ith concentration obtained using TOUGH2. The parameters e_1 and $\beta'$for the fHTE were also determined in the same manner.

3.2 Numerical results

Figures 4(a) and 5(a) show the tracer response and the temperature profile obtained from the one-layer model. The tracer response was a symmetric Gaussian distribution. This is because the tracer transport process was governed solely by advection. The solution of ADE is also plotted in Fig. 4(a). The temperature profile shows rapid thermal breakthrough. Tracer responses for the two-layer model are displayed in Fig. 4(b). In this case, the tracer responses exhibit apparently long tails and second peaks. These double-peak responses are supposed to be the result of two distinct flow pathways between the injection and production zones. The first peak in the tracer response probably was produced by the advective flow in the main conduit and the second peak was produced by the diffusion into the

surrounding rocks. Comparing Figs. 5(a) and 5(b) shows that higher permeability in the surrounding rocks reduced and delayed the temperature decline.

For the fault zone model, the permeability of the surrounding rocks according to the power law was defined as in Eq. (11). Reasonable results were obtained in the case of the index of anomalous dispersion θ over 1.0. Fig. 4(c) shows tracer responses for the fault zone model and shows that lower values of θ lead to a greater amount of diffusion of tracer into the surrounding rocks. Compared to the constant permeability distribution of the surrounding rocks (Fig. 4(b)), the spatially varying distribution of permeability produced a gradual decrease in the concentration. Several flow patterns must occur due to a wide range of permeability of surrounding rocks in the fault zone model, and the superposition of the tracer responses for each pattern may produce a gradual decrease in the concentration profile. Our results provide a clear distinction in the tracer responses and the temperature profiles between the fault zone model and the two-layer model. This suggests that a model with discontinuous permeability distribution, such as the two-layer model, is insufficient to characterize reservoir performance in a fault zone and that the spatial change in permeability must be taken into account.

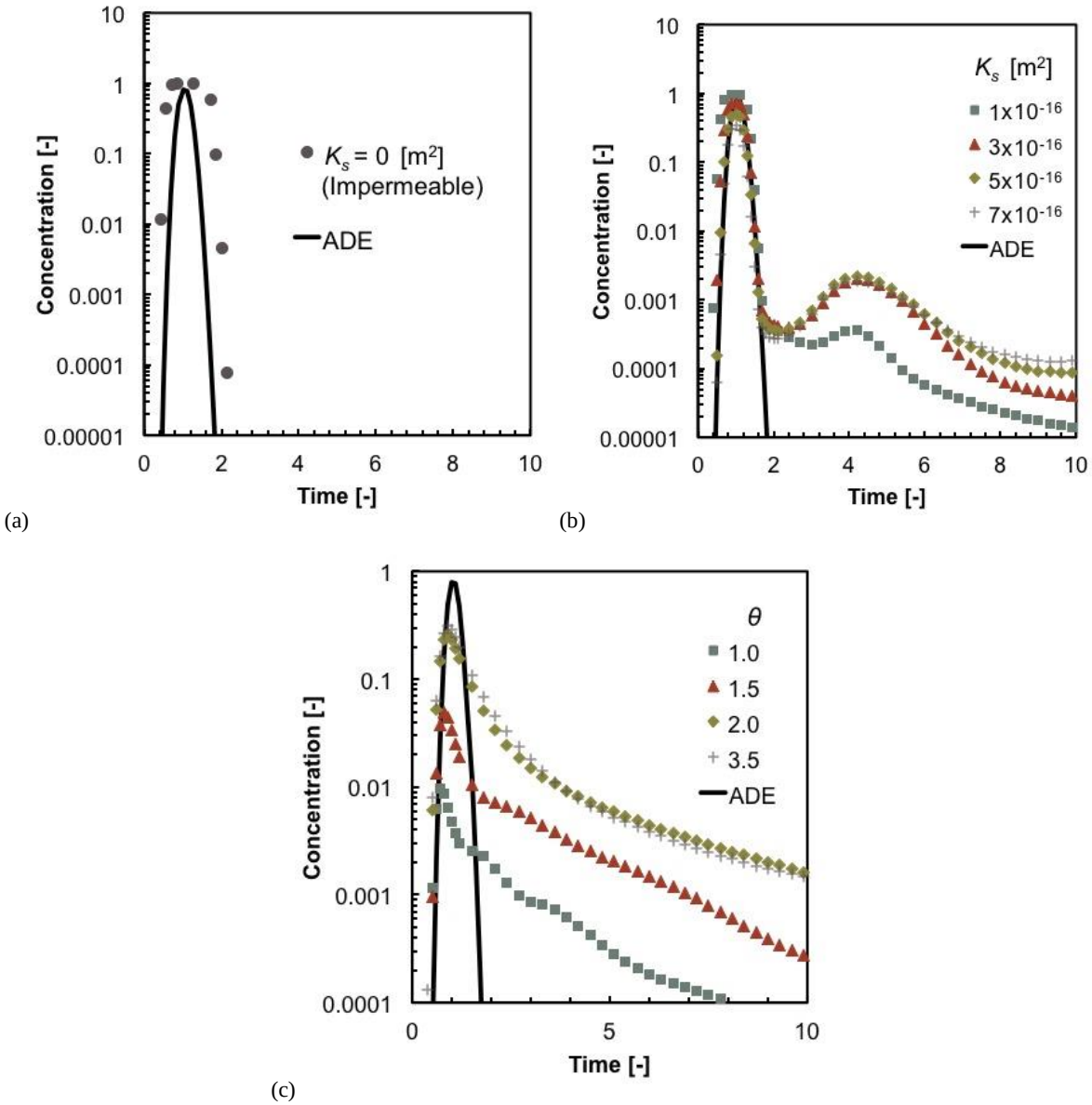

Figure 2: Effects of different permeability distributions on tracer responses calculated by TOUGH2: (a) one-layer, (b) two-layer and (c) fault zone models.

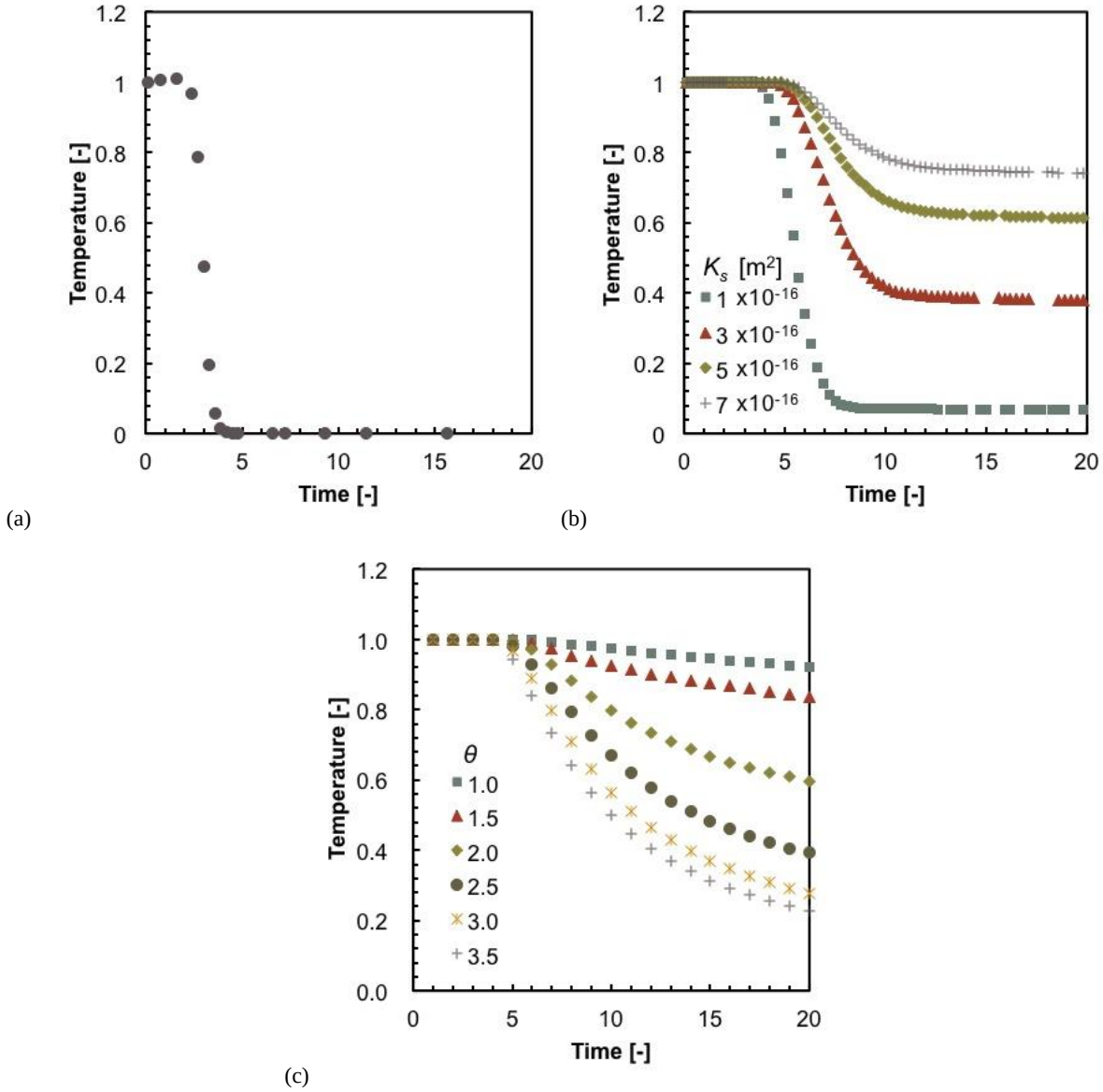

Figure 3: Effects of different permeability distributions on temperature profiles calculated by TOUGH2: (a) one-layer, (b)two-layer and (c) fault zone models.

As mentioned previously, the fADE and the fHTE have introduced the fractal diffusion coefficients of solute and heat, respectively, and can be expected to characterize tracer transport in the fault zone. The concentration and temperature results obtained using TOUGH2, which are shown in Figs. 4(c) and 5(c), were used to verify the applicability of fADE and fHTE.

Figure 4(a) shows the best-fit curves from fADE to the calculated tracer response for $\theta = 1.5$ in the fault zone model. For comparison, the best-fit curves of the conventional models are also plotted. The ADE is a conventional mass transport model and the fitting result shows a more symmetric shape, which is in disagreement with the calculated tracer response. The retardation model includes the retardation factor into the ADE, while the Fick's diffusion model takes into account the diffusion into the surrounding rock according to Fick's law. The fitting results of both models are affected by the long-term behavior but did not match the overall tracer response well. However, the fADE fitting result was in reasonable agreement with the calculated tracer response. This result corroborates that the fADE including the fractal diffusion coefficient is an appropriate model to describe tracer response in a fault zone.

Figure 4(b) shows the best-fit curves on the calculated temperature profile for $\theta = 1.5$ for the fault zone model. The basic equation for the subsurface temperature field was derived for rocks with intergranular flow by Bodvarsson (1972). Lauwerier (1955) developed an analytical solution for the heat transfer in one-dimensional flow with heat loss to confining beds according to Fick's law, and Gringarten and Sauty (1975) extended the idea to reinjection problems in geothermal fields. According to Fig. 7, the intergranular flow model is incapable of describing the temperature decline calculated by TOUGH2, in which the temperature decreased gradually due to penetration into the surrounding rocks. The fitting result obtained by the Fick's diffusion model was somewhat different from the

calculated temperature profile. The result indicates that the thermal diffusion into the surrounding rocks in the fault zone occurs more gradually than Fick's diffusion. In contrast, the fHTE was in good agreement with the temperature profile for the fault zone model. These comparisons lead us to the conclusion that the fHTE can offer an accurate evaluation of temperature profiles and an appropriate characterization of thermal response in a fault-related subsidiary structure.

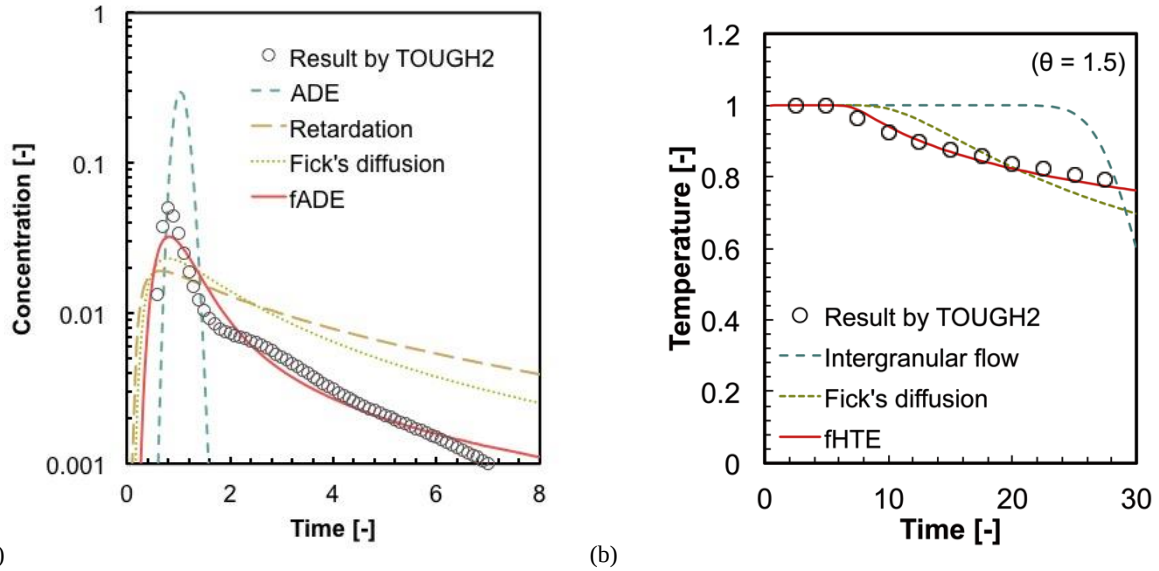

(a) (b)

Figure 4: (a) Simulated tracer response and (b) temperature profile by TOUGH2 using the fault zone model for θ = 1.5 (symbols) and best fits with the conventional models and the fADE (lines).

4. COLUMN EXPERIMENT

4.1 Experimental methods

Tracer flow experiments were designed using flow columns filled with glass beads to evaluate the effect of permeability distribution. Figure 5 illustrates the operation of the column apparatus. The fault zone model and the one-layer model were employed to evaluate the effect of permeability distribution for comparison with numerical simulations (Section 3). A 10-inch long, 3.8-inch internal diameter glass column was packed with glass beads. Different diameters of glass beads provided a spatial distribution of permeability for the fault zone model.

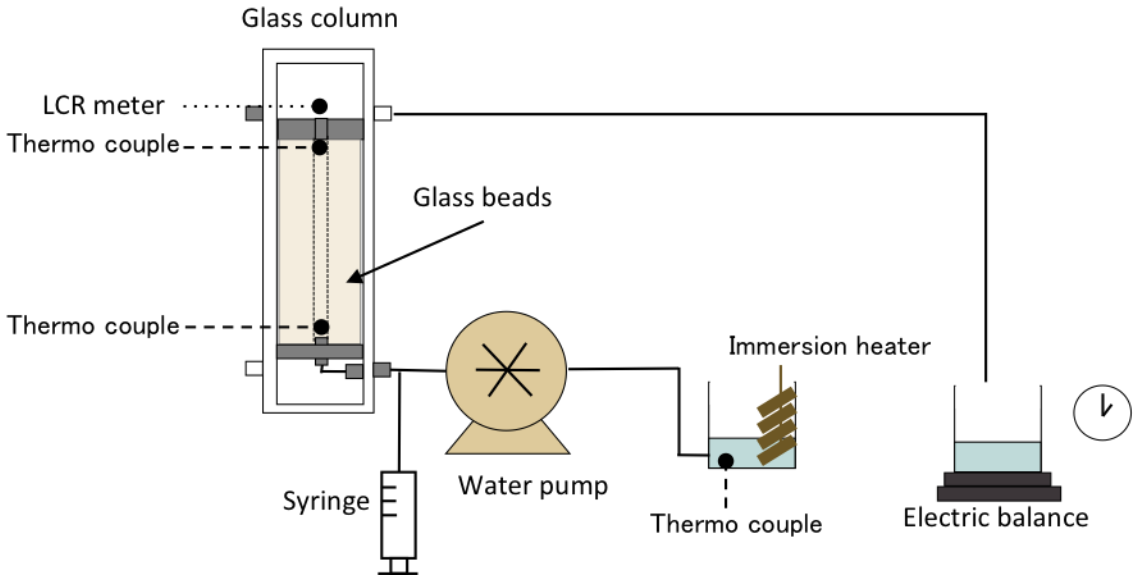

Figure 5: Experiment apparatus diagram.

Because of difficulty in creating a gradual change in permeability, the inside of the column was divided into four areas (I, II, III, and IV) each with different size of glass beads. First, thin-walled tubings were used to separate the column into the four "layers" (actually rings).

The inner diameters of the tubings were 0.25 in., 0.5 in. and 1 in., respectively. The largest glass beads were set in the innermost layer (I), while the smallest ones were allocated in the outermost layer (II). The thin wall tubing was packed with glass beads in 1-cm increments by pouring freshwater into them and pressing them down, and eventually withdrawn.

The one-layer model consists of only the innermost layer (I). The tubing with inner diameter of 0.25 in. remained in the column. The setting of glass beads and saturation for the one-layer model followed the same manner as the fault zone model.

Prior to tracer flow test, the permeability of the glass beads of different sizes was measured in a bead-filled cylinder with radius of 3.69 cm. The total amount of water flowing through the system was determined by measuring the weight of water in the exit container using a balance (Mettler balance, Model PE 300) over time. The accuracy of the balance is 0.01g.

The water head difference between the inlet and the outlet was held constant for each permeability measurement, and the flow rate was measured three times (or more) for each head difference. Measurements from three head differences in the range between 17 cm and 22 cm were used to calculate the average permeability for each glass bead size. Darcy's law for horizontal flow was utilized to compute the permeability given as:

$$K = \mu QL / \rho gAht \tag{10}$$

where Q is the volume of water [m^3], A is the surface of cylinder [m^2], t is time [s], h is the water head difference [m], L is the length of the flow path (layer of glass beads) in the cylinder [m]. μ and ρ are the viscosity and density of water. We used μ = 0.000102 [kg s m^{-2}] and ρ = 1.0 [kg m^{-3}] for water at 25 °C.

Measured permeability values were compared to theoretical values of permeability for various glass bead sizes as calculated by (Lappen et al., 1997):

$$K = \frac{D^2 \varepsilon^3}{150\ (1-\varepsilon)^2}, \tag{11}$$

where K is the permeability [m^2], D is the diameter of glass beads [m], and ε is the porosity. This study used glass beads with diameters of 0.500-0.707 mm, 0.354-0.500 mm, 0.177-0.297 mm, 0.053-0.125 mm, and 0.044-0.088mm in I, II, III, and IV areas in the column, respectively. This allocation can generate an approximate permeability distribution associated with the value of θ = 2.

For the tracer experiment, the column was saturated from below with pure water at 25 °C (room temperature). Water was injected through an injection loop using the water pump (Dynamax) from the bottom of the column. The injection rate and temperature were kept constant at 0.7 cm^3/ min and 25 °C, respectively. In this study we focused on the effect of permeability distribution on tracer response curves, so the thermal effect was neglected. The column was flushed with pure water prior to the tracer injection. The flow rate was measured over time using the balance at the outlet in the same manner as the permeability measurement.

Sodium chloride (NaCl) tracer was added to the inflow to the column as a pulse change in concentration. The experiments used a NaCl concentration of 2.5 % by weight. Concentrations of the tracer NaCl during the experiment were determined by measuring the electrical resistance of the fluid exiting the column, using a LCR meter (DE-6000-LCR, iET Labs, Inc.) at a frequency of 1 kHz.

4.2 Experimental results

The permeability of glass beads with different sizes was determined. Figure 7 illustrates the relationship between permeability and the diameters of glass beads. The measured permeability values for different glass bead diameters are plotted in Fig. 7(a) with error bars representing the standard deviation of the mean. These estimates are compared to theoretical values calculated by Eq. (11) for glass beads with porosity in the range between 0.3 and 0.4, as illustrated in Fig. 7(b). These results indicate that the measured permeability values were in reasonable agreement with the theoretical values.

Figure 8 shows the glass bead distribution in the column such that each layer (ring) contained glass beads of different diameter.

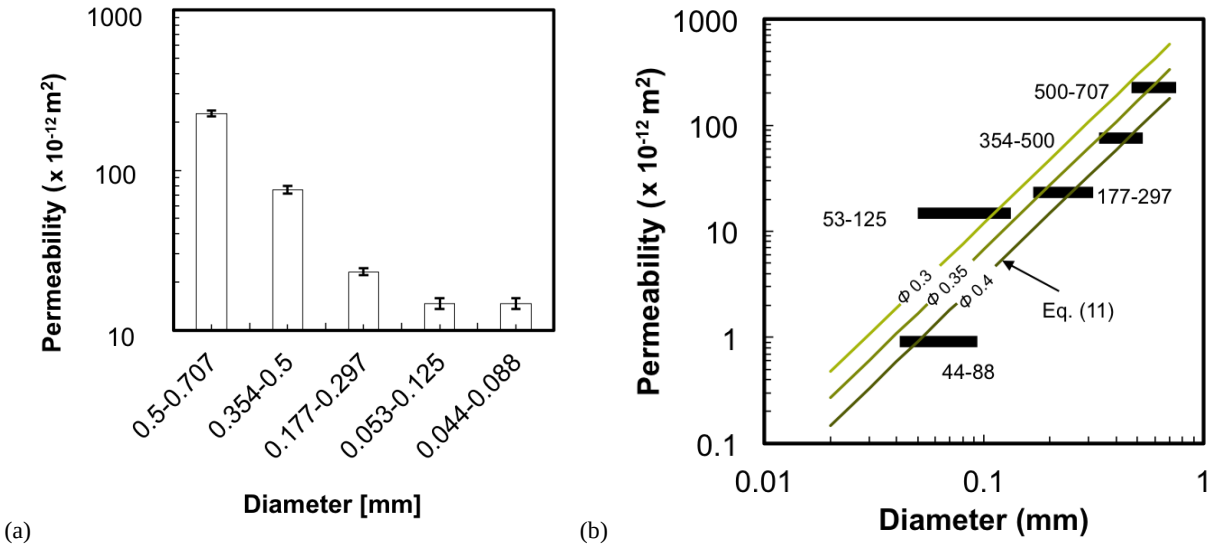

Figure 7: Measurement of permeability for glass beads with different sizes.

Figure 8: Glass bead distribution in column.

For each tracer experiment, measurements were recorded throughout the entire evolution of the tracer plume. The series resistance of the water was measured by the LCR meter at the column outlet to estimate electrical conductivity. NaCl concentration was then determined from the electrical conductivity of the solution. In our experiments, the electrical conductivity showed a power-law relation with NaCl concentration in the range from 0.01 % to 2.5 %, which was consistent with the trend in CRC Handbook of Chemistry and Physics. Concentrations were normalized by setting the background concentration to $C = 0$ and the injected concentration of 2.5% to $C = 1$. Breakthrough curves were plotted as normalized concentration versus time graphs. Measurement error in the curve includes the sensitivity of the resistance measurement.

A concentration profile for the one-layer model is illustrated in Figs. 9(a) and (b). Figures 9(a) and (b) display the linear plot and semilog plot, respectively. The curve shows a sharp peak at early time. This is consistent with the numerical result shown in Fig. 2(a). The result indicates that the tracer transport process was governed solely by advection. On the other hand, Figs. 9(c) and (d) show tracer responses for the fault-zone model using different sizes of glass beads. Compared to the constant permeability distribution for the one-layer model, a more gradual decrease in the concentration was observed. This result is also consistent with the numerical simulation result shown in Fig. 2(c).

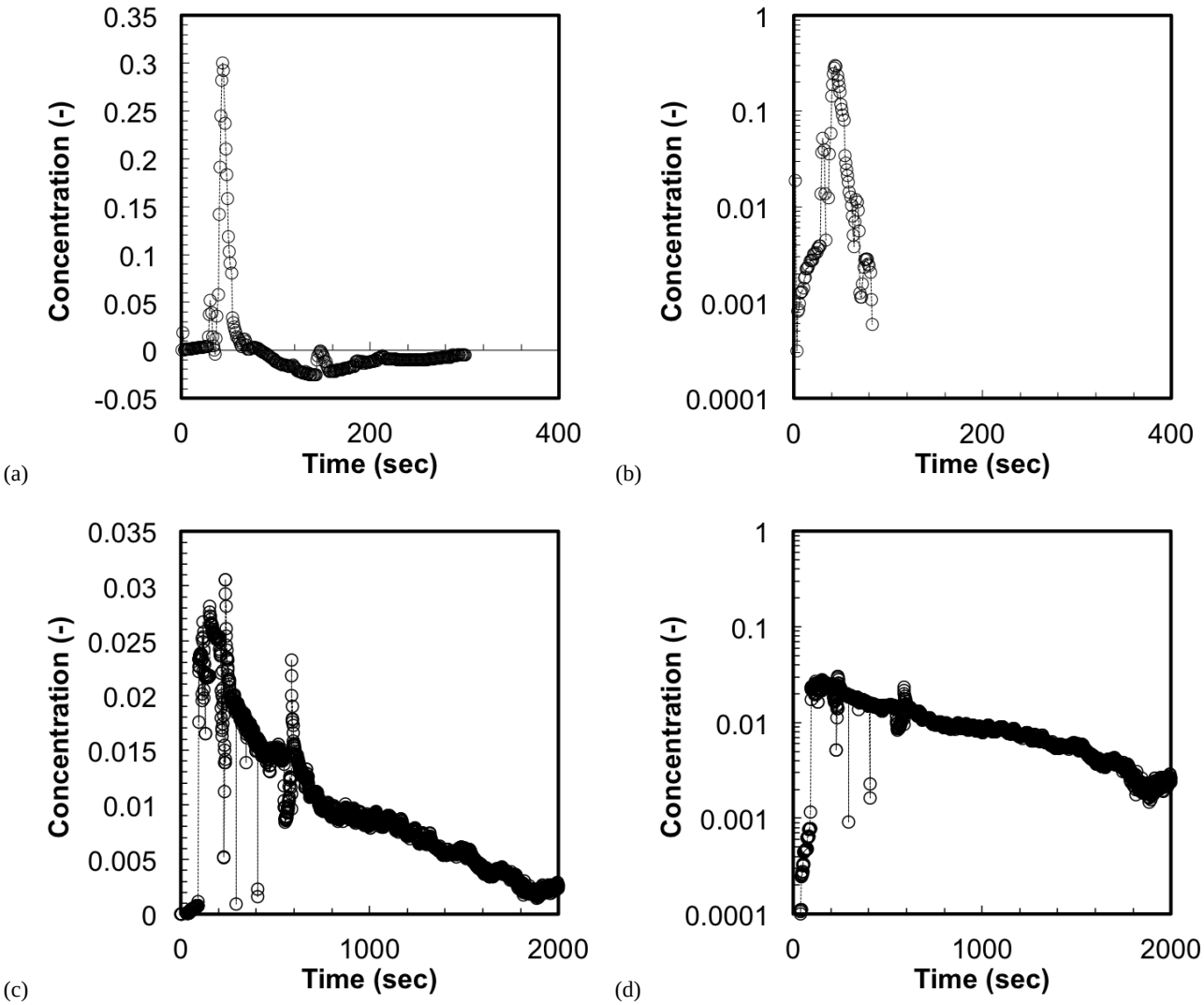

Figure 9: Tracer breakthrough curves in column experiment: (a) linear plot and (b) semi-log plot for the one-layer model and (c) linear plot and (d) semi-log plot for the fault zone model.

5. DISCUSSION AND CONCLUSIONS

Numerical simulations and column flow tests were conducted to generate tracer responses and temperature profiles. The results revealed how permeability patterns in the surrounding rocks affect the reservoir performance. Both numerical and experimental results simulating tracer response with a fault-related structure produced gradual decrease in the concentration of tracer. This resulted from a distribution in which permeability values decayed with distance from the main conduit.

Conventional advection-dispersion models can describe tracer and thermal responses accurately only for impermeable surrounding rocks. An increase in the permeability of the surrounding rocks led to a long tail in the tracer response and a more gradual decline in the temperature history. One of the models with a discontinuous permeability distribution produced a tracer response including two peaks. Thus, the spatial change in permeability should be taken account in cases where the tracer response shows a gradual decline. The fADE solution was found to be in agreement with the tracer response for a fault zone model that incorporated decays in permeability with distance from the main conduit (as simulated in TOUGH2). Curve fitting with the temperature profile suggested that the fHTE can be used to characterize temperature profiles in fractured media.

The column experiment generated only the tracer response in a fault related structure. Future work will address the effect of the structure on the thermal behavior, which can provide insight about prediction of the occurrence of thermal breakthrough and temperature decline around fault zones.

The fractal diffusion coefficient taken into account in the fADE declines with distance from a main conduit and therefore was consistent with the actual diffusion process in a fault-related subsidiary structure. The fADE can summarize the complexity based on fractal geometry and can analyze mass transport in a fractured reservoir quickly and efficiently. Our previous study has demonstrated that the

fADE offers a method for predicting tracer responses irrespective of well intervals in a fractured reservoir (Suzuki et al., 2012). Future developments from this study will include prediction of thermal breakthrough for different well intervals and optimization of the well location and/or the condition of reinjection.

ACKNOWLEDGEMENTS

This research was supported by JSPS Postdoctoral Fellowships for Research Abroad (H26-416).

REFERENCES

Agosta F, Kirschner DL. Fluid conduits in carbonate-hosted seismogenic normal faults of central Italy. J Geophys Res 2003;108 (B4): doi:10.1029/2002JB002013.

Aksoy N, Serpen U, and Filiz Ş. Management of the Balcova–Narlidere geothermal reservoir, Turkey. Geothermics 2008; 37(4): 444–66.

Axelsson G.Sustainable geothermal utilization – Case histories; definitions; research issues and modeling. Geothermics 2010; 39: 283–91.

Barenblatt GI, Zheltov YP, Kochina IN. Basic concepts in the theory of seepage of homogeneous liquids in fissured rocks. J of Appl Math Mech 1960; 24(5): 1286–303.

Bear J. Dynamics of Fluids in Porous Media. New York: American Elsevier; 1972.

Benson DA, Wheatcraft SW, Meerschaert MM. Application of a fractional Advection-Dispersion Equation. Water Resour Res, 36(6), (2000), 1403–1412.

Bodvarsson G. Thermal problems in siting of reinjection wells. Geothermics 1972; 1(2): 63–66.

Bodvarsson G, Tsang CF. Injection and thermal breakthrough in fractured geothermal reservoirs. J Geophys Res 1982; 87: 1031–48.

Bonnet E, Bour O, Odling NE, Davy, P, Main, I, Cowie, P et al. Scaling of fracture systems in geological media, Rev Geophys 2001; 39: 347–83.

Brock WG, Engelder JT. Deformation associated with the movement of the Muddy Mountain overthrust in the Buffington window. southeastern Nevada. Geol Soc Am Bull 1997; 88: 1667–77.

Brogi A. Fault zone architecture and permeability features in siliceous sedimentary rocks. Insights from the Rapolano geothermal area (Northern Apennines, Italy). J Struct Geol 2008; 30: 237–56.

Bullivant DP, Sullivan MJO, Mechanics A, Zealand N. Matching a field tracer test with some simple models Water Resour Res 1989; 25: 1879–91.

Caine J, Evans J, Forster C. Fault zone architecture and permeability structure. Geology 1996; 24: 1025–8.

Chester JS, Chester FM, Kronenberg AK. Fracture surface energy of the Punchbowl fault, San Andreas system, Nature 2005; 437: 133–6.

Chester FM, Logan JM. Implications for mechanical properties of brittle faults from observations of the Punchbowl Fault Zone. California. Pure Appl Geophys 1986; 124: 79–106.

Coats KD, Smith BD. Dead-end pore volume and dispersion in porous media. SPE J 1964; 4: 73-84.

De Joussineau G, Aydin A. The evolution of the damage zone with fault growth in sandstone and its multiscale characteristics. J Geophys Res 2007; 112: doi: 10.1029/2006JB004711.

Evans JP, Forster CB, Goddard JV. Permeability of fault-related rocks, and implications for hydraulic structure of fault zones. J Struct Geol 1997; 19: 1393-404.

Faulkner DR, Jackson CAL, Lunn RJ, Schlische RW, Shipton ZK, Wibberley CAJ et al. A review of recent developments concerning the structure, mechanics and fluid flow properties of fault zones. J Struct Geol 2010; 32(11): 1557-75.

Fomin SA, Chugunov VA, Hashida T. The effect of non-Fickian diffusion into surrounding rocks on contaminant transport in a fractured porous aquifer. Phil Trans R Soc A 2005; 461: 2923–39.

Fomin SA, Chugunov VA, Hashida T. Non-Fickian mass transport in fractured porous media. Adv Water Resour 2011; 34: 205–14.

Gringarten AC, Sauty JP. A theoretical study of heat extraction from aquifers with uniform regional Flow. J Geophys Res 1975; 80(35): 4956-62.

Gudmundsson A. Rock Fractures in Geological Processes. 1st ed. Cambridge University Press: New York; 2011.

Kaya E, Zarrouk SJ, O'Sullivan MJ. Reinjection in Geothermal Fields: A Review of Worldwide Experience. Renew Sust Energ Rev 2011; 15(1): 47–68.

Kocabas I. Geothermal reservoir characterization via thermal injection backflow and interwell tracer testing. Geothermics 2004; 34(1): 27–46.

Lappan RE, Hrymak AN., Pelton R. Dependence of in situ precipitate deposition on flow characteristics in multi-permeability porous media, Chemical Engineering Science, 1997: 52(17), 2963-2975.

Lauwerier HA. The transport of heat in an oil layer caused by the injection of hot fluid. J App Sci Res 1955: 5 (2–3): 145-50.

Le Garzic E, de L'Hamaide T, Diraison M, Geraud Y, Sausse J, de Urreiztieta M et al. Scaling and geometric properties of extensional fracture systems in the proterozoic basement of Yemen. Tectonic interpretation and fluid flow implications. J Struct Geol 2011; 33: 519–36.

Massart B, Paillet M, Henrion V, Sausse J, Dezayes C, Genter A, et al. Fracture Characterization and stochastic modeling of the granitic basement in the HDR Soultz project (France). Proc WGC, Bali, Indonesia 2010.

Mitchell TM, Faulkner DR. The nature and origin of off-fault damage surrounding strike-slip fault zones with a wide range of displacements: a field study from the Atacama fault system, northern Chile. J Struct Geol 2009: 31: 802–16.

Pruess K, Narasimhan TN. On fluid reserves and the production of superheated steam from fractured, vapor-dominated geothermal Reservoirs. J Geophys Res 1982; 87(B11): 9329-39.

Pruess K, Narasimhan TN. A practical method for modeling fluid and heat flow in fractured porous media. SPE J 1985: 25(1); 14-26.

Pruess K, Oldenburg C, Moridis G. TOUGH2 user's guide, version 2.0. LBL Report 1999: LBNL-43134.

Samko, SG, Kilbas, AA, Marichev, OI. Fractional integrals and derivatives: theory and applications. London: Gordon and Breach; 1993.

Savage H, Brodsky E. Collateral damage: Evolution with displacement of fracture distribution and secondary fault strands in fault damage zones J Geophys Res 2011; 116(B3): B03405.

Shook GM. Predicting thermal breakthrough in heterogeneous media from tracer tests, Geothermics, 30, (2001), 573-89.

Suzuki A, Makita H, Niibori Y, Fomin SA, Chugunov VA, Hashida T. Analysis of water injection in fractured reservoirs using a fractional-derivative-based mass and heat transfer model. Math Geosci 2014: doi: 10.1007/s11004-014-9522-5.

Suzuki A, H, Niibori Y, Fomin SA, Chugunov VA, Hashida T. Prediction of reinjection effects in fault-related subsidiary structure by using fractional derivative-based mathematical model fo r sustainable design of geothermal reservoirs. Geothermics 2015 (Submitted for publication).

Warren JE, Root PJ. The behavior of naturally fractured reservoirs. SPE J 1963; 3: 245–55.

Welty J,Wicks CE, Rorrer GL,Wilson RE. Fundamentals of momentum, heat andmass transfer. 5th ed. New York: Wiley; 2007.

Woods, AW, Fitzgerald, SD. The vaporization of a liquid front moving through a hot porous rock, J Fluid Mech 1993; 251: 563-79.

Zhang, Y, Benson, DA, Reeves, DM. Time and Space Nonlocalities underlying fractional-derivative Models: distinction and literature review of field applications. Adv Water Resour 2009; 32(4): 561–81.

Zhang X, Lv M, Crawford JW, Young IM. The impact of boundary on the fractional advection–dispersion equation for solute transport in soil: Defining the fractional dispersive flux with the Caputo derivatives. Adv Water Resour 2007: 30; 1205–17..